Influence of wall modes on the onset of bulk convection in a rotating cylinder

F. Marques[1] and J. M. Lopez[2]
[1]*Departament de Física Aplicada, Universitat Politècnica de Catalunya, 08034 Barcelona, Spain*
[2]*Department of Mathematics and Statistics, Arizona State University, Tempe, Arizona 85287, USA*

(Received 21 June 2007; accepted 7 January 2008; published online 28 February 2008)

The onset of thermal convection in an enclosed rotating cylinder is greatly influenced by the interaction between the Coriolis force and the cylinder sidewall. For temperature differences between the hot bottom and the cool top that are too small to sustain convection throughout the entire cylinder, convection sets in as pairs of wall-bounded hot thermal plumes ascend and cold thermal plumes descend in the sidewall boundary layer, the so-called wall modes of rotating convection. Over an extensive range of parameter space, several wall modes with different numbers of thermal pairs coexist stably, and this multiplicity of states leads to very rich nonlinear dynamics as the temperature difference is increased to a level supporting thermal convection throughout the bulk of the cylinder. The bulk convection takes on characteristics of Küppers–Lortz spatiotemporal chaos, but its interaction with the persistent wall modes also leads to further flow complications which are explored here via numerical simulations. © *2008 American Institute of Physics*.
[DOI: 10.1063/1.2839340]

I. INTRODUCTION

Onset of bulk convection in rotating cylinders in the limit of zero centrifugal force has been of great interest due to the presence of spatiotemporal chaos right at the onset of convection.[1] In unbounded rotating convection, the Küppers–Lortz (KL) instability[2] is a primary source of spatiotemporal chaos. It is an instability of a parallel roll state to rolls oriented at another angle, which in turn are unstable to rolls oriented at yet another angle, and so on, leading to interesting time-dependent behavior. States with these characteristics have been observed in experiments in finite cylinders.[3–10] In spite of this, there are many open questions associated with the onset of bulk rotating convection. To begin with, since the KL-type instabilities have thus far only been studied theoretically in the absence of lateral boundaries, one can only surmise how their behavior will change in finite containers.[11] The expectation has been that in containers of sufficiently large radius-to-height aspect ratios, KL-type dynamics will persist. Recently however, bulk convective states with locally square plan forms have been observed experimentally and computed numerically very close to onset.[12,13] These states do not appear to have any relationship with the predictions from the unbounded theory[14,15] and their origin remains poorly understood.

Confined rotating convection introduces new phenomena which have no counterpart in unbounded rotating convection, such as the wall modes which result from the interaction between the Coriolis force and the cylinder sidewall.[5,16–19] The presence of wall modes leads to a large multiplicity of coexisting stable states via the Eckhaus–Benjamin–Feir (EBF) instability,[20–22] and the onset of bulk convection when the Coriolis force is sufficiently large is influenced by the EBF instability of the wall modes.

The experimental investigation of the EBF instability of the wall modes was facilitated by the fact that the azimuthal wavenumber of the wall mode m varies with the system rotation rate, and by preparing a wall mode with a certain m at a rotation rate higher or lower than that desired and then changing the rotation to the desired rate provided a mechanism to produce wall modes with a range of m at the same parameter values. The experiments also used the influence of the bulk convective mode on the wall modes. The length scale of the bulk convection varies with Rayleigh number (Ra) and so one can induce wall modes with different azimuthal wavenumbers m by driving the system into the bulk convection regime at some high Ra value and then quickly reducing to a desired lower Ra to obtain a pure wall mode with m influenced by the bulk convection length scale.[21]

The influence of rotation rate, and the high Ra excursions into the bulk convection regime, on the selection of the wall mode wavenumber has been used very effectively experimentally. However, how the azimuthal wavenumber m of the wall mode influences the transition to bulk convection when increasing Ra has not been investigated systematically. The nature of this transition is not well understood presently. The phenomenological description from experiments characterizes the transition as a continuous process to aperiodic time-dependent convection as Ra is increased, signaled by a marked increase in the slope of the linear relationship between the heat transport (i.e., the Nusselt number Nu) and the Rayleigh number.[5,23] The current view is that since there is no appreciable amplitude of the wall mode in the central portion of the cylinder, the bulk convection can grow from small amplitude despite being a secondary transition. Experimentally, it is observed that the bulk convection and wall modes are spatially separated and only interact weakly. This view is further justified since the onset of bulk convection occurs at Rayleigh numbers very close to the critical Rayleigh numbers determined by linear stability analysis in an

unbounded layer over a wide range of rotation rates,[24] and the critical length scale also agrees.[25,26] Nevertheless, near onset of bulk convection, it has been experimentally observed that the boundary forcing from the wall mode has a significant effect on the KL switching frequency of the bulk convection.[7]

There are other interesting aspects of the transition that have been observed experimentally. For example, for a range of Ra near the onset of bulk convection, the flow pattern consists of axisymmetric rings in the middle region, surrounded by a wall mode pattern near the cylinder wall.[25]

The main goal of this paper is to analyze the influence of the wall modes in the transition to bulk convection. In order to do this, we have computed 24 different wall modes at Prandtl number $\sigma=7.0$ in a cylinder of radius-to-depth aspect ratio $\gamma=4$ rotating with Coriolis number $\Omega=625$ at Rayleigh number $\mathrm{Ra}=9.0\times10^4$ (see Sec. II for the definitions of the parameters). In such a system, bulk convection sets in at about $\mathrm{Ra}=9.6\times10^4$. These wall modes have azimuthal wavenumbers $m\in[10,33]$, and their Eckhaus–Benjamin–Feir instabilities at lower Ra were previously investigated.[22] Here, we have used these wall mode states at $\mathrm{Ra}=9.0\times10^4$ as initial conditions at $\mathrm{Ra}=10^5$ and have evolved the initial value problem out to at least 30 thermal time units, by which time the bulk convective states are established. The flow near the sidewall maintains the fast precessing wall mode structure essentially unaffected by the convective motions in the interior, but the form of the interior bulk convection is greatly influenced by the wall mode. For wall modes with azimuthal wavenumbers m near the extremes of the EBF-stable range, cellular structures with fourfold symmetry persist for long times. These are very much like the square patterns that have been observed experimentally[12] and numerically computed.[13] For most m values however, the bulk convection consists of roll-like structures with KL dynamics.

II. GOVERNING EQUATIONS AND NUMERICAL SCHEME

We consider the flow in a circular cylinder of radius r_0 and depth d, rotating at a constant rate ω rad/s. The top endwall is maintained at a constant temperature $T^*=T_0-0.5\Delta T$ and the bottom endwall at a constant temperature $T^*=T_0+0.5\Delta T$. The Boussinesq approximation is implemented, which treats all fluid properties as constant, except for the density in the gravitational buoyancy term. The centrifugal buoyancy term is not considered here. It has not been considered in most of the theoretical analysis we are comparing with, and most of the experiments are designed to minimize it. To lowest order, the density varies linearly with temperature, i.e.,

$$\rho=\rho_0[1-\alpha(T^*-T_0)], \tag{1}$$

where T_0 is the mean temperature and ρ_0 is the density at that temperature.

The system is nondimensionalized using d as the length scale, d^2/κ as the time scale, where κ is the thermal diffusivity, and ΔT as the temperature scale. There are four nondimensional parameters:

$$\text{Rayleigh number:}\quad \mathrm{Ra}=\alpha g d^3\Delta T/\kappa\nu,$$

$$\text{Coriolis number:}\quad \Omega=\omega d^2/\nu,$$

$$\text{Prandtl number:}\quad \sigma=\nu/\kappa,$$

$$\text{Aspect ratio:}\quad \gamma=r_0/d,$$

where g is the gravitational acceleration, α is the coefficient of volume expansion, and ν is the kinematic viscosity.

The nondimensional cylindrical domain is $(r,\theta,z)\in[0,\gamma]\times[0,2\pi)\times[-1/2,1/2]$. The nondimensional governing equations in the rotating frame of reference are

$$(\partial_t+\mathbf{u}\cdot\nabla)\mathbf{u}=-\nabla p+\sigma\nabla^2\mathbf{u}+\sigma Ra T\hat{z}+2\sigma\Omega\mathbf{u}\times\hat{z}, \tag{2}$$

$$(\partial_t+\mathbf{u}\cdot\nabla)T=\nabla^2T,\quad \nabla\cdot\mathbf{u}=0, \tag{3}$$

where $\mathbf{u}$ is the velocity field, $T=T^*-T_0$ is the temperature deviation with respect to the mean temperature, p is the dynamic pressure which incorporates the hydrostatic pressure due to the gravitational and centrifugal forces, and $\hat{z}$ is the unit vector in the vertical direction z.

The boundary conditions for $\mathbf{u}$ and T are

$$r=\gamma:\quad T_r=u=v=w=0, \tag{4}$$

$$z=\pm1/2:\quad T=\mp0.5,\quad u=v=w=0, \tag{5}$$

where (u,v,w) are the components of $\mathbf{u}$ in cylindrical coordinates. Regularity conditions on the axis $(r=0)$ are enforced using appropriate spectral expansions for $\mathbf{u}$ and T.

The governing equations have been solved using a pseudospectral second order time-splitting method, that was used to study the EBF instability of the wall modes.[22] We have used the wall modes that were computed at $\mathrm{Ra}=9\times10^4$, with $m\in[10,33]$ as initial conditions to study the onset of bulk convection as Ra is increased. As in Ref. 22, we fix $\gamma=4$, $\sigma=7.0$, and $\Omega=625$, and consider variations in Ra. We have used 24 spectral modes in z, 48 in r, 184 in θ and a time step $dt=2\times10^{-5}$ thermal time units.

A useful characteristic of the solutions obtained is the kinetic energy in the mth Fourier mode of the solution

$$E_m=\frac{1}{2}\int_{z=-1/2}^{z=1/2}\int_{r=0}^{r=\gamma}\boldsymbol{u}_m\cdot\bar{\boldsymbol{u}}_m r\mathrm{d}r\mathrm{d}z, \tag{6}$$

where $\mathbf{u}_m$ is the mth Fourier mode of the velocity field. It aids in monitoring the relative influence and switching between different modes during temporal evolution.

III. BACKGROUND

A numerical study of the onset of thermal convection in a rotating circular cylinder with the same parameter values as in the present work was previously performed[22] for Ra values well below the onset of bulk modes. Here we present a brief summary of those results. The onset of thermal convection is to wall modes which consist of a periodic array of alternating hot and cold thermal plumes confined to a thin boundary layer at the cylinder sidewall, forming an essentially one-dimensional pattern characterized by the number

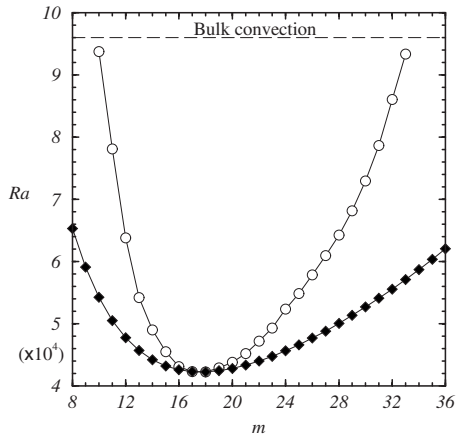

FIG. 1. Stability diagram for wall modes with azimuthal wavenumber m, showing the marginal stability curve (♦) and the Eckhaus–Benjamin–Feir curve (○) for $\Omega=625$, $\sigma=7$, $\gamma=4$.

of hot/cold plume pairs, m. These states are born in symmetry-breaking supercritical Hopf bifurcations at the marginal stability curve (solid curve with ♦ in Fig. 1), but only the rotating wave with $m=18$ is born stable; the other rotating waves stabilize in a sequence of secondary Hopf bifurcations, in a process analogous to the sequence of pitchfork bifurcations in a Ginzburg–Landau equation model.[27] The wall mode pattern typically precesses retrograde with respect to the rotation of the cylinder. For temperature differences greater than critical, a number of distinct wall modes, distinguished by m, coexist and are stable. Their dynamics are controlled by an Eckhaus–Benjamin–Feir (EBF) instability.

Figure 1 shows the marginal stability curve (♦) for the Hopf bifurcation from the base state to rotating waves with different azimuthal wavenumbers $m\in[8,36]$. The curve has a minimum at $m=18$, $\mathrm{Ra}_w\approx 42,286$. Figure 1 also includes the Eckhaus–Benjamin–Feir stability curve (○), where the various wall modes born on the marginal stability curve become stable with increasing Ra following a number of secondary Hopf bifurcations. Of course, although we talk about curves, both the marginal stability curve and the EBF curve are in fact loci of discrete points since the azimuthal wavenumber m is an integer.

For $\Omega>70$, the onset of bulk convection in a rotating cylinder is not always to an expected KL state, but rather has been observed to consist of patterns of plumes arranged with fourfold symmetry within patches.[12] These patterns have been observed to persist for long times very close to onset. In the experiments,[12] the squares persist at $\epsilon_b=(\mathrm{Ra}-\mathrm{Ra}_b)/\mathrm{Ra}_b\approx 0.091$ (where Ra_b is the critical Ra for the onset of bulk convection), whereas for slightly larger $\epsilon_b=0.14$ the square patterns are observed only intermittently. It is significant that the squares at onset have been observed experimentally for $\Omega>70$. It is for $\Omega>70$ that the onset of convection as Ra is increased is first to a wall mode, and the onset of bulk convection is a secondary bifurcation at higher Ra.

IV. RESULTS

The onset of bulk convection is at approximately $\mathrm{Ra}_b\approx 9.6\times 10^4$, very close to the linear estimate[24] for the onset of two-dimensional rolls in a horizontally periodic layer between no-slip isothermal plates rotating with $\Omega=625$, $\mathrm{Ra}_\infty\approx 9.2\times 10^4$. Ra_b is also very close to the onset of axisymmetric target pattern convection from the conduction state, when the dynamics is restricted to the axisymmetric ($m=0$) subspace,[28] $\mathrm{Ra}_{\mathrm{axisym}}\approx 9.85\times 10^4$.

We have computed 26 different wall modes with azimuthal wavenumbers $m\in[10,35]$ at $\mathrm{Ra}=9.0\times 10^4$, all within the EBF curve in Fig. 1 and therefore stable, except for the last two ($m=34$ and 35). These wall mode states at $\mathrm{Ra}=9.0\times 10^4$ have been used as initial conditions at $\mathrm{Ra}=10^5$ and these initial value problems have been evolved out to at least 30 thermal time units, by which time the bulk convective states are well established. As in the experiments,[12] our investigation is very close to the onset of bulk convection, with $\epsilon_b\approx 0.04$. In contrast to most experimental studies however, the rotation in our problem is much faster with $\Omega=625$ [in Ref. 12, $\Omega\in(70,180)$]. A consequence of a larger Ω is that the bulk convection sets in at a value of Ra much greater than that for the wall modes. In our computational study, $\epsilon=(\mathrm{Ra}_b-\mathrm{Ra}_w)/\mathrm{Ra}_w\approx 1.36$, whereas in the experiments of Ref. 12, ϵ is small (it is not specified in their paper, but similar experiments in Ref. 21 report that ϵ varies linearly with Ω from $\epsilon=0$ at $\Omega\approx 70$ to $\epsilon\approx 0.2$ at $\Omega\approx 200$). This means that the wall modes are quite weak in the experimental studies near the onset of bulk convection. Furthermore, with the large Ω in our study, the EBF-stable band of wall modes (for a given cylinder aspect ratio) is much wider at the onset of bulk convection. In the present study, the EBF band extends from $m=10$ to $m=33$ at Ra_b, providing wall modes varying in size by more than a factor of 3.

Figure 2 shows isotherms at the mid-depth horizontal plane of six different convective states after 30 thermal time units, between $m=12$ and $m=32$ in steps of four. In all cases ($m\in[10,33]$), the flow near the sidewall maintains the fast precessing wall mode structure, essentially unaffected by the convective motions in the interior. In particular, the presence of bulk convection does not change the azimuthal wavenumber m of the wall mode.

Figure 3 shows the precession frequencies of the wall modes at $\mathrm{Ra}=10^5$, as a function of the azimuthal wavenumber m of the wall modes, with well developed bulk convection (filled symbols). The precession frequencies of the pure wall modes (open symbols), for Ra below the onset of bulk convection have been included for comparison. The precession frequencies of the wall modes are not modified by the presence of the bulk convection, and follow the same trend as for the pure wall modes.

There is a narrow annular transitional region between the wall mode and the bulk convection. From the isotherms (Fig. 2), we see that the form of the interior bulk convection is greatly influenced by the wall mode. For wall modes with small azimuthal wavenumber m, in particular for $m=12$ and 14, cellular structures with fourfold symmetry can be observed. Typically, for larger m the bulk convection consists

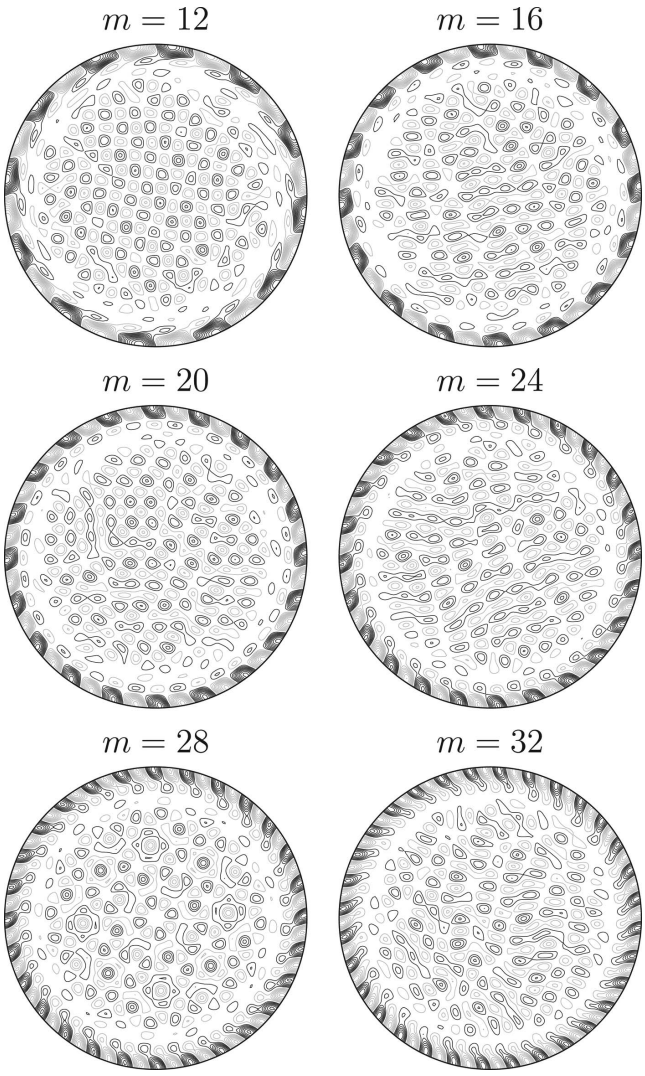

FIG. 2. Isotherms at mid-depth at Ra=10^5, computed with initial conditions corresponding to pure wall modes at Ra=9×10^4 with wavenumber m as indicated (all at Ω=625, σ=7.0, and γ=4).

of roll-like aligned structures showing spatial defects and small regions with different cellular structures. All of these states have erratic temporal characteristics. In a couple of cases we have continued the states to lower Ra nearer to the onset of the bulk convection from the uniformly precessing wall mode state and have found that the erratic temporal

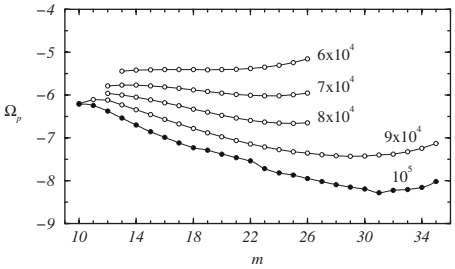

FIG. 3. Precession frequencies of the wall modes at Ra=10^5, as a function of the azimuthal wavenumber m of the wall modes, with well developed bulk convection (filled symbols) and of the pure wall modes (open symbols) for Ra as indicated.

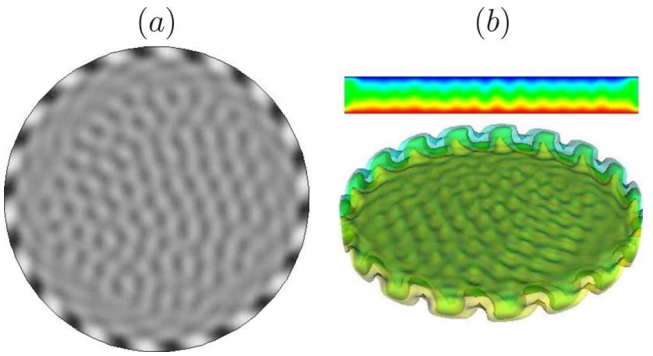

FIG. 4. (Color online) Bulk convective state at Ra=10^5, γ=4, σ=7.0, and Ω=625, started from a wall mode with m=18 at Ra=9.0×10^4; (a) shows gray-scaled isotherms at midheight and (b) shows a perspective view of the same solution with three isolevels of temperature and the temperature in a meridional cut $r\in[-\gamma,\gamma]$, $z\in[-0.5,0.5]$ (enhanced online).

behavior persists all the way to onset at about Ra=9.6×10^4. These results agree with the reported chaos from the onset, with Küppers–Lortz dynamics, but also show the presence in some cases of squares, that have been observed to be the dominant behavior at smaller rotation rates.[12,13]

Figure 4 shows gray-scaled isotherms at midheight and a perspective view of the same solution with three isolevels of temperature and the temperature in a meridional cut $r\in[-\gamma,\gamma]$, $z\in[-0.5,0.5]$ of a bulk convective state at Ra $=10^5$, γ=4, σ=7.0, and Ω=625, started from a wall mode with m=18 at Ra=9.0×10^4. The online videos show the temporal evolution of these still-shots over a few precession periods of the wall mode component of the flow at a slow enough frame-rate for the precession to be smooth in the videos, and so the slow bulk dynamics are barely apparent.

Figure 5 shows the variation of the Nusselt number with the Rayleigh number for the 24 solutions analyzed. The dependence is linear both for the pure wall modes and also for the bulk convective states, but there is a sharp increase in the slope at the onset of the bulk convection. Nu is time-independent for the wall modes (they are rotating waves), but it is time-dependent (in fact chaotic) for the bulk convection states; time averages over several thermal time units are plotted in the figure. This is in very good agreement with the experiments,[21] who also report a linear dependence Nu(Ra)

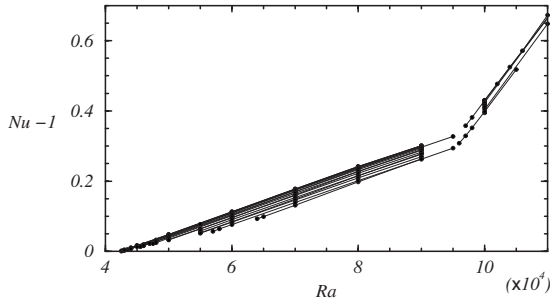

FIG. 5. Nusselt number vs Rayleigh number for γ=4, σ=7.0, and Ω=625. The first part of the linear dependence corresponds to wall modes with $m\in[10,33]$, and Nu is time-independent; for the second part, only a few branches are shown and Nu is temporally chaotic and time averages over several thermal time units are plotted.

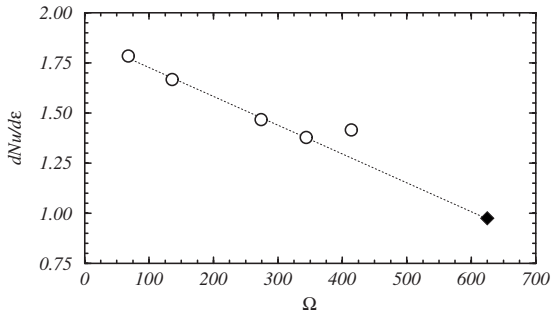

FIG. 6. Slope $(d\mathrm{Nu}/d\epsilon)_b$ vs Ω. ◆ is our computed result at $\gamma=4$, $\sigma=7.0$, and $\Omega=625$. ○ are the experimental values (Ref. 21) at $\gamma=5$, $\sigma=6.7$, and Ω as indicated.

for both states. The slopes in Fig. 5 have been measured as $d\mathrm{Nu}/d\epsilon$, where $\epsilon=\mathrm{Ra}/\mathrm{Ra}_w-1$ is the relative variation of Ra from the onset of wall mode convection, for comparison purposes. The average slope for the wall modes, averaged over the 24 cases considered $(m\in[10,33])$ is $(d\mathrm{Nu}/d\epsilon)_w=0.269\pm0.004$. We have also computed the slope for bulk convection, $(d\mathrm{Nu}/d\epsilon)_{Ab}=0.975$. Figure 6 shows this value and the experimentally measured slopes[21] $(d\mathrm{Nu}/d\epsilon)_b$ at lower rotation rates, for $\sigma=6.7$ and $\gamma=5$. The figure shows a linear variation of $(d\mathrm{Nu}/d\epsilon)_b$ with Ω, and only a weak dependence on the aspect ratio γ.[21]

Next, we describe in detail the transition from wall modes to bulk convection, and the characteristics of the flow when the bulk convection is well established, for selected m values.

Figure 7 shows the time evolution of the Nusselt number for the $m=12$ case, for $t\in[20,50]$ (in thermal units), when the bulk convection is well established. The time average of this signal is the Nusselt number value plotted in Fig. 5 at $\mathrm{Ra}=10^5$ for $m=12$. The signal shows small chaotic variations along with time intervals where it is almost constant. Snapshots of the flow at $t=30$, 40, and 50 are shown in Fig. 8. All of them exhibit the presence of an array of square cells filling the bulk of the flow, with defects in several regions taking the form of alignments of three or four cells in a straight roll. The square cells in this $m=12$ case persist for all computed times (up to $t=50$ thermal units). The chaotic behavior of the time series corresponds to the formation and destruction of straight rolls in different regions of the domain. The online video (Fig. 8) is an animation of this for $t\in[20,50]$ at 5 frames per time unit, showing the dynamics of the bulk convection (however, the precession of the wall mode component is too fast to be temporally resolved in the video at this frame rate).

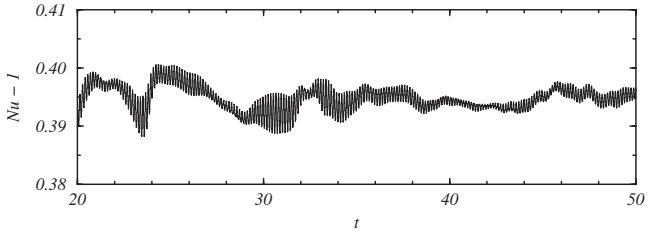

FIG. 7. Time evolution of the Nusselt number, beginning with a wall mode solution with $m=12$ at $\mathrm{Ra}=9\times10^4$ and impulsively changing to $\mathrm{Ra}=10^5$ at $t=0$ (time is in thermal units).

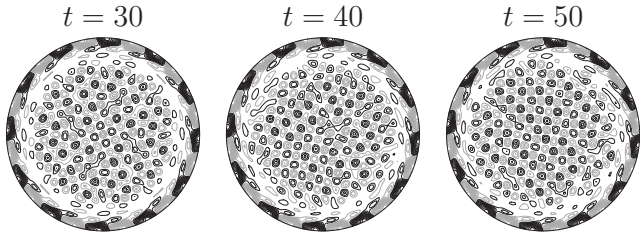

FIG. 8. Isotherms at mid-depth at various times, following an impulsive increase in Ra to 10^5 from an initial condition corresponding to an $m=12$ wall mode at $\mathrm{Ra}=9\times10^4$ (enhanced online; video shows the evolution from $t=20$ to $t=50$ at 5 frames per time unit).

Figure 9 shows the time evolution of the Nusselt number for the $m=13$ case, for $t\in[0,30]$. There is a long transient of about 15 thermal times for the evolution from the pure wall mode $(t=0)$ to sustained bulk convection. Figure 10 shows snapshots of this flow every 5 thermal time units. The first two pictures show the development of the flow in the bulk. The wall mode induces spiral perturbations that penetrate into the bulk (up to $t=5$). The time series of the Nusselt number (Fig. 9) shows a regular large amplitude modulation associated with this phase. Along the spiral rolls circular convective plumes develop, and the spirals start to break down, resulting in a large number of plumes organized in concentric circles $(t=10)$ resembling a Rosetta window. In the middle of the cylinder, a target pattern appears, formed by concentric circular rolls. This transient axisymmetric pattern has been observed in experiments.[25] This initial transitional stage is followed by a time interval, for $t\in[15,24]$, where the convective cells organize themselves in a square pattern, very similar to the square pattern in the $m=12$ case. Both the Nusselt time series (compare Figs. 7 and 9) and the isotherms at mid-depth (compare Figs. 8 and 10) bear strong similarities during this phase. However, for subsequent times $(t>25)$, the square pattern is replaced by Küppers–Lortz-type dynamics: The convection cells organize in straight parallel rolls unstable to rolls oriented to another angle, and the pattern shows patches of 4–6 straight parallel rolls that change orientation in time, with rolls in different patches having different orientations, as illustrated in the snapshot at $t=30$ in Fig. 10 and animated in the online video at 5 frames

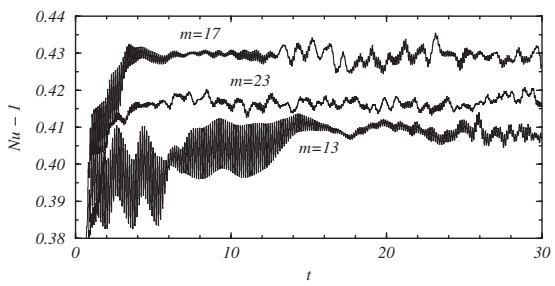

FIG. 9. Time evolution of the Nusselt number, for various initial conditions consisting of a wall mode solution with m as indicated at $\mathrm{Ra}=9\times10^4$ and impulsively changing to $\mathrm{Ra}=10^5$ at $t=0$ (time is in thermal units).

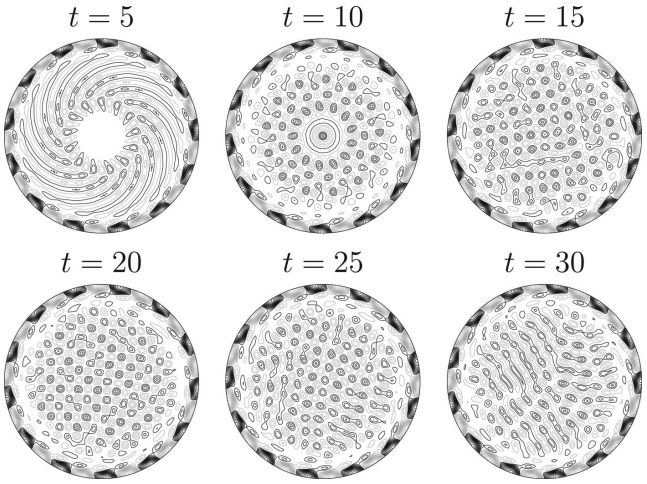

FIG. 10. Isotherms at mid-depth at various times, following an impulsive increase in Ra to 10^5 from an initial condition corresponding to an $m=13$ wall mode at $\mathrm{Ra}=9\times10^4$ (enhanced online; video shows this temporal evolution at 5 frames per time unit).

per time unit. This KL chaotic dynamics persist indefinitely, and its signature in the Nusselt number time series takes the form of chaotic oscillations (see Fig. 9 for $t>25$).

Figure 9 also shows the time evolution of the Nusselt number for the $m=17$ case, for $t\in[0,30]$, Fig. 11 shows snapshots of this flow at different times, and the online video is an animation of the evolution at 5 frames per time unit. In this case we can distinguish four different stages. First of all, for $t\in[0,3)$ we observe the transitional stage from wall modes to bulk convection, which is shorter than in the previous example, and instead of developing axisymmetric target patterns near the center of the cylinders, there is a symmetric circular region with azimuthal wavenumber 3 (see the snapshot at $t=2$). For $t\in[3,10)$, the convective cells organize themselves in an hexagonal pattern, with the typical defects in the form of alignments of several cells in straight rolls (snapshots at $t=3$ and 5). After this hexagonal stage, a square pattern forms and persists for $t\in[10,15)$ (snapshots at $t=10$ and 15). At later times, the chaotic Küppers–Lortz pattern develops, and persist for all the times considered (up to $t=30$).

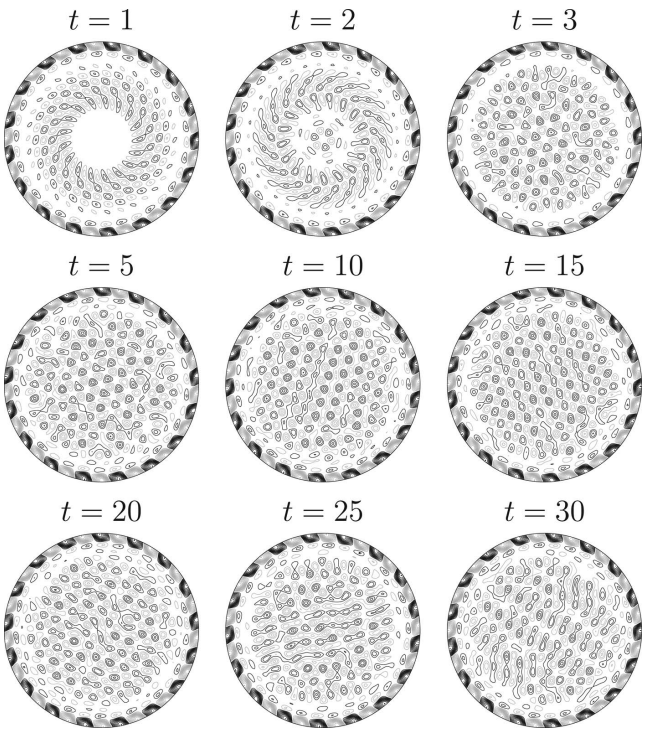

FIG. 11. Isotherms at mid-depth at various times, following an impulsive increase in Ra to 10^5 from an initial condition corresponding to an $m=17$ wall mode at $\mathrm{Ra}=9\times10^4$ (enhanced online; video shows this temporal evolution at 5 frames per time unit).

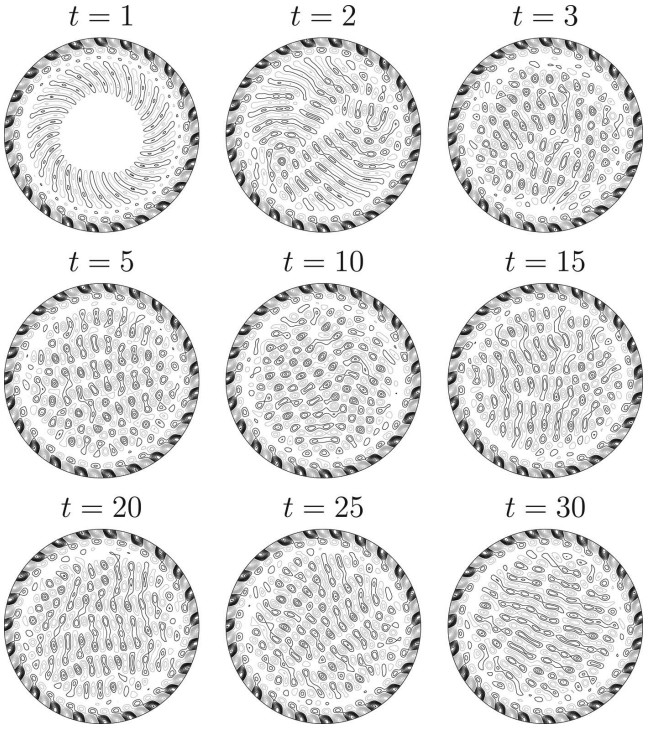

FIG. 12. Isotherms at mid-depth at various times, following an impulsive increase in Ra to 10^5 from an initial condition corresponding to an $m=23$ wall mode at $\mathrm{Ra}=9\times10^4$ (enhanced online; video shows this temporal evolution at 5 frames per time unit).

Figure 9 also shows the time evolution of the Nusselt number for the $m=23$ case, for $t\in[0,30]$. In this case the transitional stage is very short, and we cannot distinguish different stages in the development of bulk chaotic dynamics. This is confirmed by looking at the snapshots of the flow at different times in Fig. 12, and the online video is an animation of the evolution at 5 frames per time unit. The spirals emanating from the wall boundary layer at $t=1$ break down very quickly without forming symmetric structures (see snapshot at $t=2$). The resulting disordered straight rolls organize in patches of straight parallel rolls that change orientation in time, the chaotic Küppers–Lortz-type dynamics, that persists for $t\geqslant3$. The corresponding Nusselt number time series (Fig. 9) has the typical aperiodic structure associated with Küppers–Lortz dynamics with propagating defects, that we have also observed in the late time evolution of most other cases.

The different dynamics we have observed in the previous examples are typical and are present in most of the 24

cases examined. There is always an initial transitional stage from wall mode to bulk convection, and a late stage for large enough time characterized by chaotic Küppers–Lortz-type patterns, with the exception of the $m=12$ and 31 cases, where the Küppers–Lortz-type patterns do not develop, at least in the time span considered (up to 50 viscous times). Between these two stages, different forms of well developed bulk chaotic dynamics may appear, including square and hexagonal patterns. What changes from one case to another is the nature and time span of the different stages. They also differ in the details of the initial transition from wall modes to developed bulk convection, presenting in some cases symmetric patches near the center of the cylinder; we have observed axisymmetric target patterns, and patches with azimuthal wavenumber 3.

For $m \leqslant 20$ there is always a complex transitional intermediate stage involving patterns with symmetry: Squares, hexagonal or axisymmetric. For $m > 20$ the evolution is from spirals to a KL dynamics, skipping the intermediate stage.

The wall mode structure does not change during the whole evolution, and continues precessing steadily, except near the EBF boundary at large m-values, as will be discussed in the next section. The precession period is about two orders of magnitude shorter than the time scale of the bulk mode dynamics. Most of the time, there is also a clear spatial separation between the wall mode and bulk dynamics, but defects originating in this annular region propagate into the bulk and influence its dynamics. In particular, the precession of the structures in the bulk (square patterns, etc.) is not uniform but rather erratic, due to the defects induced by the wall modes that penetrate quickly into the bulk at an irregular rate. For slower rotation rates Ω, with much weaker wall modes than in the present computations, this effect may not be so important, and regularly precessing square patterns have been observed.[12]

V. BULK-INDUCED EBF INSTABILITIES

For large m-values, close to the EBF curve (see Fig. 1), the onset of bulk convection may trigger changes in the azimuthal wavenumber of the wall mode. Figure 13 shows one of these changes. Starting with a pure $m=31$ stable wall mode at $\mathrm{Ra}=9\times10^4$ as an initial condition for a run at $\mathrm{Ra}=10^5$, after two thermal times by which the bulk convection has been established, the azimuthal wavenumber of the wall mode changes to $m=29$. Figure 13(a) shows a sudden jump in the Nusselt number at this time, associated with the change in m. Figure 13(b) shows the evolution of the modal kinetic energies associated with the dominant modes, further illustrating the switching between the wall modes $m=31$ and 29. These changes are strongly dependent on the initial conditions, i.e., the specific perturbations introduced in the initial conditions. Different evolutions and final states can be reached using different perturbations. The transition illustrated in Fig. 13 corresponds to the introduction of a small perturbation (of relative strength of 10^{-6}) in the azimuthal mode $m=1$ at $t=0$.

Figure 14 shows isotherms at mid-depth of the transition $m=31\rightarrow29$ in Fig. 13; the two snapshots are at times $t=1.92$ and 2.00. In the first snapshot, two pairs of diametrically opposed plumes (at about 1 and 7 o'clock) shrink to a smaller size than the other plumes, and in the second snapshot they have been absorbed by the adjacent plumes, that become thicker than the rest. Then there is a readjustment period, from about $t=2$ to $t=2.5$ during which the wall plumes adjust their size and a uniform $m=29$ wall mode component emerges. The spiral in the center of the isotherms in Fig. 14 is due to the $m=1$ perturbation used to induce the transition. By about $t=3$, bulk convection similar to the snapshots shown in Fig. 2 has fully developed, with square patterns persisting for a long time.

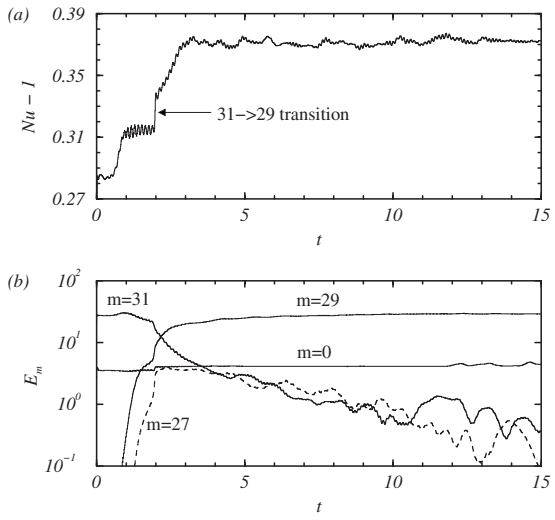

FIG. 13. Time evolution of (a) the Nusselt number and (b) the dominant modal energies corresponding to an initial $m=31$ wall mode at $\mathrm{Ra}=10^5$.

Changes in the azimuthal wavenumber of the wall mode have been observed starting with wall modes outside the EBF-stable band. These wall modes are easily obtained numerically by restricting the computations to the appropriate subspace, and experimentally could be produced at larger Ra numbers, where they are stable, and then reduce Ra to the desired value, where they are unstable. These wall modes persist for long times before decaying to different wall modes inside the EBF band. Figure 15 shows the transitions in azimuthal wavenumber that an initial $m=35$ wall mode undergoes. The computation starts with a pure $m=35$ wall mode; after two thermal times bulk convection is established,

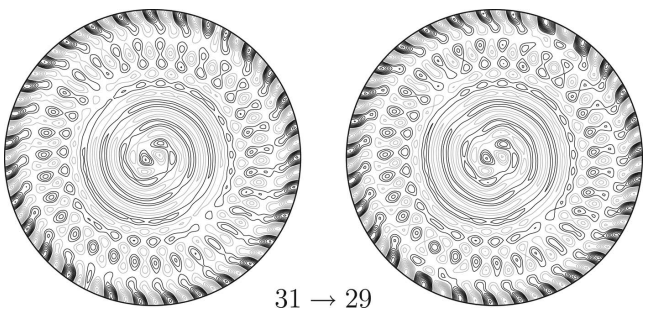

FIG. 14. Isotherms at mid-depth of the transition $m=31\rightarrow29$ of an $m=31$ initial wall mode at $\mathrm{Ra}=10^5$, as indicated in Fig. 13.

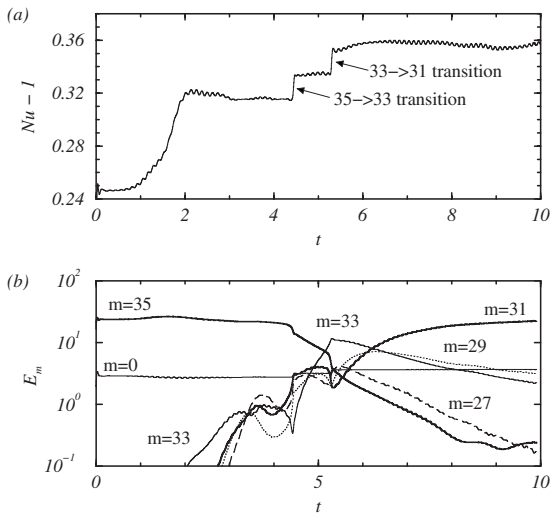

FIG. 15. Time evolution of (a) the Nusselt number and (b) the dominant modal energies corresponding to an initial $m=35$ wall mode at $\mathrm{Ra}=10^5$.

and the unstable $m=35$ wall mode persists up to $t\approx 4.4$, when it decays to a $m=33$ wall mode, which in turn decays to a $m=31$ wall mode in another thermal time. This stable $m=31$ wall mode persists for subsequent times.

The transitions $m=35\rightarrow 33$ and $m=33\rightarrow 31$ appear as sudden jumps in the Nusselt number time series in Fig. 15(a), as in the $m=31$ case previously examined, suggesting that the Nusselt number is a very good variable with which to monitor the evolution of these complex states. Figure 15(b) shows the evolution of the modal kinetic energies associated with the dominant Fourier modes; the correlation with the jumps in Nusselt number is very good. Figure 16 shows isotherms at mid-depth of the two transitions $m=35\rightarrow 33$ and $m=33\rightarrow 31$. In both cases the transition consists of

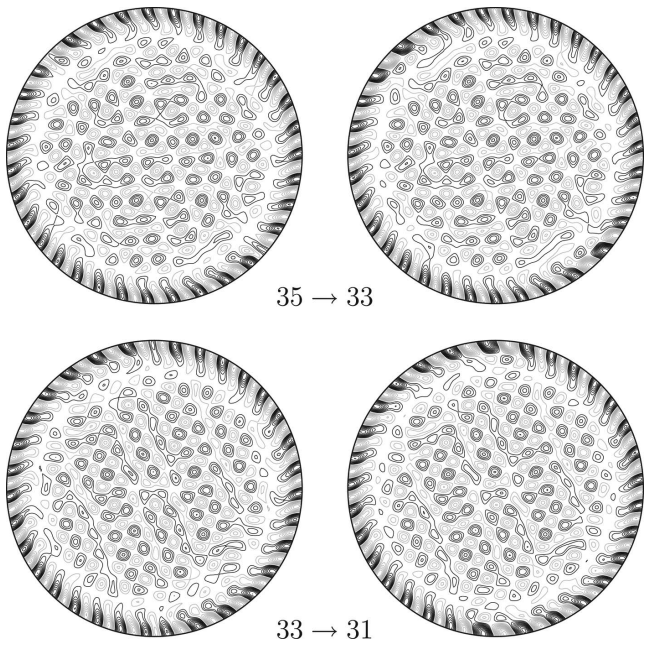

FIG. 16. Isotherms at mid-depth of the transitions $m=35\rightarrow 33$ and $m=33\rightarrow 31$ of an $m=35$ initial wall mode at $\mathrm{Ra}=10^5$, as indicated in Fig. 15.

two pairs of diametrically opposed thermal plumes at the wall weakening and being absorbed by adjacent plumes. In the transition $m=35\rightarrow 33$ this occurs at about 4 and 10 o'clock, and in the transition $m=33\rightarrow 31$ it happens at about 12 and 6 o'clock in the snapshots shown. It is interesting to notice in Fig. 16 that by the time the jump $m=33\rightarrow 31$ takes place, the bulk convection has developed a square pattern that persists for a long time.

The details of the transitions are very much dependent on the nature of the initial conditions. The basins of attraction of the large variety of states (primarily characterized by the m of the wall mode component, as well as by the spatiotemporal patterns of the bulk convection) are expected to be very complicated. The unstable modes that result from the sequences of secondary Hopf bifurcations leading to the EBF-stable band of wall modes number 141 for $m\in[10,33]$ in the problem we have investigated ($m_c=18$, and each wall mode undergoes $|m-m_c|$ secondary Hopf bifurcations in order to become stable). These unstable modes are modulated rotating waves and form parts of the boundaries of the basins of attractions of the wall modes. As Ra is increased beyond Ra_b, this complicated intertwined and fractal network of basin boundaries makes it very difficult (if not impossible) to provide general rules for the transitions between modes, and is at the heart of the extreme sensitivity to initial conditions observed.

VI. DISCUSSION AND CONCLUSIONS

The transition from wall mode convection to bulk convection is difficult to characterize, in large part due to the multiplicity of finite amplitude states that are competing. The bulk convective state one observes depends very much on initial conditions. In this paper, we have detailed what happens in a very specific region of parameter space, but these are typical examples rather than peculiar examples. Careful experiments (e.g., see Refs. 1, 21, and 26, and references therein) covering larger regions of parameter space report very similar behavior to that observed in this study. If the computations at $\mathrm{Ra}=10^5$ are initiated with the trivial conductive state plus very small random perturbations, the flow that evolves corresponds to a bulk convection with Küppers–Lortz dynamics coupled to a uniformly precessing wall mode with azimuthal wavenumber of about $m=20$ (the precise value of m is sensitive to the initial small perturbations). On the other hand, if the computation for $\mathrm{Ra}=10^5$ involves a quasistatic increase in Ra from small values below the onset of the wall modes, then the final state has the $m=18$ wall mode as it is the first to bifurcate from the conduction state at the parameter values considered here. Yet, if the initial condition is another one of the wall modes that are Eckhaus–Benjamin–Feir stable, then the state arrived at for $\mathrm{Ra}=10^5$ typically retains that wall mode, regardless of whether Ra is impulsively or slowly increased to 10^5. In this study, we have systematically examined the fate of 24 such initial conditions, corresponding to wall modes with $m\in[10,33]$ at $\mathrm{Ra}=9\times 10^4$ and analyzed the bulk convective states that result at $\mathrm{Ra}=10^5$.

The early transients from initial conditions corresponding to wall modes with $m \leqslant 20$ always show a spiral structure penetrating into the bulk from the wall mode, followed by a complex transitional stage involving competition between different kinds of patterns (squares, hexagons, concentric rings) and eventually evolving into a chaotic Küppers–Lortz-type dynamics. The case with $m=12$ is an exception, where the square pattern persists for a long time (at least 50 viscous times). For $m>20$ the evolution is directly from spirals to a Küppers–Lortz dynamics, skipping the intermediate stage. What emerges from these simulations is that we are not dealing with a typical simple bifurcation scenario, but rather with a complex interplay between several bifurcations and many coexisting states.

It is already known from previous studies[22,27] that inside the Eckhaus–Benjamin–Feir stable region, not only is there a large multiplicity of rotating waves (the pure wall modes), but there are also a larger number of unstable quasiperiodic solutions (mixed wall modes) born at the secondary Hopf bifurcations that stabilize the wall modes. Additional complex solutions also exist, coming from nearby codimension-two and higher bifurcations, resulting from the simultaneous occurrence of some of the aforementioned bifurcations. This large multiplicity of coexisting states is in sharp contrast with the ideal scenario for the onset of Küppers–Lortz dynamics, where straight rolls bifurcate in an infinite horizontal fluid layer, and periodicity is assumed and imposed in both horizontal directions. Although the Küppers–Lortz behavior is dominant in the bulk at large Ω and large containers, the periodic assumption fails to incorporate endwall effects, and in fact the limit of finite containers with aspect ratio going to infinity is a singular limit that does not converge to the periodic case; this situation is similar to the problem in resolving endwall effects and the infinite aspect-ratio limit in Taylor–Couette flow, which has been shown to be a singular limit.[29–31]

In this context of complex bifurcational processes for the onset of bulk convection, the presence of other complex patterns such as squares, hexagons, and target patterns should not be a surprise. These patterns usually appear only as transient states reflecting the competition between the multiplicity of existing solutions, but for particular parameter values they may become the dominant permanent pattern, as is the case with squares at $\Omega=625$ for the $m=12$ wall mode and for lower Ω values.[12]

Experiments from Bajaj *et al.*[12] reports that for $\Omega>70$ the bifurcation remains supercritical, but the onset of the convective pattern has no similarity to the expected KL state. Instead, the pattern consists of cells which are usually arranged so as to have local fourfold coordination. They also note that for $\Omega>70$, the onset of convection as Ra is increased is first to a wall mode and then with further increase in Ra the bulk mode bifurcates from the wall mode. From their Fig. 6, perfect squares persist for very small $\epsilon \sim 0.091$ (at $\epsilon \sim 0.14$, the patterns are erratic with intermittent regular square cell patterns that precess).

All of our computations are at $\epsilon \approx (100\,000 - 96\,000)/96\,000 \approx 0.04$, also very close to the onset of the bulk mode from the wall mode. But we have two major differences with the experiments: Faster rotations, our $\Omega = 625$, whereas their $\Omega \in (70, 180)$, and perhaps more importantly, our wall modes are much more established with $\epsilon_w \approx (100\,000 - 42\,286)/42\,286 \approx 1.36$, whereas their ϵ_w is small (not specified in the paper, but similar experiments from Liu and Ecke[21] show that $\epsilon_w \approx 0.2$ for $\Omega \approx 200$. These differences may account for our square patterns not precessing regularly like the ones observed in Ref. 12).

Idealizations in fluid dynamics have been, and continue to be, very useful in order to gain understanding of the dynamics of the physical system. Restriction to an axisymmetric subspace has played an important role in the early stages of analysis, and the assumption of periodic infinite domains has resulted in the comprehensive program summarized by the *Busse balloon* and in the discovery of the Küppers–Lortz instability. But these are idealizations, and when dealing with the details of a real problem, in a finite container, the inclusion of realistic boundary conditions is essential. Generally, in fluid dynamics, this results in a nonlinear systems of PDEs requiring direct numerical simulations. Of course aspects of the idealized problem manifest themselves to a greater or lesser degree in the full problem. We have seen this in this study where typically the bulk convection takes on Küppers–Lortz-type dynamics.

ACKNOWLEDGMENTS

Stimulating discussions on the physics and numerics of this problem with O. Batiste, I. Mercader, and A. Meseguer are very much appreciated. This work was supported by the National Science Foundation Grant No. DMS-0505489, the Spanish Ministry of Education and Science Grant No. FIS2004-01336, and Catalonian Government Grant No. SGR-00024. Computational resources of ASU's Fulton HPCI are greatly appreciated.

[1] E. Bodenschatz, W. Pesch, and G. Ahlers, "Recent developments in Rayleigh–Bénard convection," Annu. Rev. Fluid Mech. **32**, 709 (2000).
[2] G. Küppers and D. Lortz, "Transition from laminar convection to thermal turbulence in a rotating fluid layer," J. Fluid Mech. **35**, 609 (1969).
[3] F. H. Busse and K. E. Heikes, "Convection in a rotating layer: A simple case of turbulence," Science **208**, 173 (1980).
[4] J. J. Niemela and R. J. Donnelly, "Direct transition to turbulence in rotating Bénard convection," Phys. Rev. Lett. **57**, 2524 (1986).
[5] F. Zhong, R. Ecke, and V. Steinberg, "Asymmetric modes and the transition to vortex structures in rotating Rayleigh–Bénard convection," Phys. Rev. Lett. **67**, 2473 (1991).
[6] F. Zhong and R. Ecke, "Pattern dynamics and heat transfer in rotating Rayleigh–Bénard convection," Chaos **2**, 163 (1992).
[7] L. Ning and R. E. Ecke, "Küppers–Lortz transition at high dimensionless rotation rates in rotating Rayleigh–Bénard convection," Phys. Rev. E **47**, R2991 (1993).
[8] Y. Hu, R. Ecke, and G. Ahlers, "Time and length scales in rotating Rayleigh–Bénard convection," Phys. Rev. Lett. **74**, 5040 (1995).
[9] Y. Hu, R. E. Ecke, and G. Ahlers, "Convection under rotation for Prandtl numbers near 1: Linear stability, wave-number selection, and pattern dynamics," Phys. Rev. E **55**, 6928 (1997).
[10] Y. Hu, W. Pesch, G. Ahlers, and R. E. Ecke, "Convection under rotation for Prandtl numbers near 1: Küppers–Lortz instability," Phys. Rev. E **58**, 5821 (1998).
[11] E. Knobloch, "Rotating convection: Recent developments," Int. J. Eng. Sci. **36**, 1421 (1998).
[12] K. M. S. Bajaj, J. Liu, B. Naberhuis, and G. Ahlers, "Square patterns in Rayleigh–Bénard convection with rotation about a vertical axis," Phys. Rev. Lett. **81**, 806 (1998).

[13] J. J. Sánchez-Álvarez, E. Serre, E. Crespo del Arco, and F. H. Busse, "Square patterns in rotating Rayleigh–Bénard convection," Phys. Rev. E **72**, 036307 (2005).
[14] R. M. Clever and F. H. Busse, "Nonlinear properties of convection rolls in a horizontal layer rotating about a vertical axis," J. Fluid Mech. **94**, 609 (1979).
[15] T. Clune and E. Knobloch, "Pattern selection in rotating convection with experimental boundary conditions," Phys. Rev. E **47**, 2536 (1993).
[16] R. E. Ecke, F. Zhong, and E. Knobloch, "Hopf-bifurcation with broken reflection symmetry in rotating Rayleigh–Bénard convection," Europhys. Lett. **19**, 177 (1992).
[17] H. F. Goldstein, E. Knobloch, I. Mercader, and M. Net, "Convection in a rotating cylinder. Part 1. Linear theory for moderate Prandtl numbers," J. Fluid Mech. **248**, 583 (1993).
[18] E. Y. Kuo and M. C. Cross, "Traveling-wave wall states in rotating Rayleigh–Bénard convection," Phys. Rev. E **47**, R2245 (1993).
[19] J. Herrmann and F. H. Busse, "Asymptotic theory of wall-attached convection in a rotating fluid layer," J. Fluid Mech. **255**, 183 (1993).
[20] Y. Liu and R. E. Ecke, "Eckhaus–Benjamin–Feir instability in rotating convection," Phys. Rev. Lett. **78**, 4391 (1997).
[21] Y. Liu and R. E. Ecke, "Nonlinear traveling waves in rotating Rayleigh–Bénard convection: Stability boundaries and phase diffusion," Phys. Rev. E **59**, 4091 (1999).
[22] J. M. Lopez, F. Marques, I. Mercader, and O. Batiste, "Onset of convection in a moderate aspect-ratio rotating cylinder: Eckhaus–Benjamin–Feir instability," J. Fluid Mech. **590**, 187 (2007).
[23] F. Zhong, R. Ecke, and V. Steinberg, "Rotating Rayleigh–Bénard convection: Asymmetric modes and vortex states," J. Fluid Mech. **249**, 135 (1993).
[24] S. Chandrasekhar, *Hydrodynamic and Hydromagnetic Stability* (Oxford University Press, Oxford, 1961).
[25] L. Ning and R. E. Ecke, "Rotating Rayleigh–Bénard convection: Aspect-ratio dependence of the initial bifurcations," Phys. Rev. E **47**, 3326 (1993).
[26] R. E. Ecke and Y. Liu, "Traveling-wave and vortex states in rotating Rayleigh–Bénard convection," Int. J. Eng. Sci. **36**, 1471 (1998).
[27] L. S. Tuckerman and D. Barkley, "Bifurcation analysis of the Eckhaus instability," Physica D **46**, 57 (1990).
[28] J. M. Lopez, A. Rubio, and F. Marques, "Traveling circular waves in axisymmetric rotating convection," J. Fluid Mech. **569**, 331 (2006).
[29] T. B. Benjamin and T. Mullin, "Notes on the multiplicity of flows in the Taylor experiment," J. Fluid Mech. **121**, 219 (1982).
[30] A. Lorenzen and T. Mullin, "Anomalous modes and finite-length effects in Taylor–Couette flow," Phys. Rev. A **31**, 3463 (1985).
[31] A. S. Landsberg and E. Knobloch, "Oscillatory bifurcation with broken translation symmetry," Phys. Rev. E **53**, 3579 (1996).